



# In-situ synthesis and binding of silver nanoparticles to dialdehyde and carboxylated cellulose nanofibrils, and active packaging therewith

Mohamed Aouay · Roberto J. Aguado · Genís Bayés · Núria Fiol · Jean-Luc Putaux · Sami Boufi · Marc Delgado-Aguilar

Received: 4 December 2023 / Accepted: 17 April 2024  
© The Author(s) 2024

**Abstract** The present work reveals the potential application of dialdehyde and carboxylated nanocellulose for the in-situ reduction of  $\text{Ag}^+$  and immobilization as silver nanoparticles (AgNPs) on cellulose surfaces. Tollens' reagent ( $\text{Ag}(\text{NH}_3)_2\text{OH}$ ) at concentrations ranging from  $5 \cdot 10^{-3}$  to  $10^{-1}$  M was incorporated in both dialdehyde cellulose (DAC) and dialdehyde-modified TEMPO-oxidized cellulose nanofibers (DA-TOCNFs). The results showed that DA-TOCNFs facilitated faster reduction of  $\text{Ag}^+$  and effective immobilization of AgNPs on the nanocellulose surface. The resulting suspensions exhibited

stability and demonstrated strong antimicrobial activity against *Bacillus subtilis* when coated on paper surfaces. Importantly, the coated papers did not show significant silver migration to food simulants B (3 vol% acetic acid) and D1 (ethanol/water mixture, 50 vol%), indicating the potential of these suspensions for active food packaging. The advantages of using DA-TOCNFs over DAC were attributed to their higher cationic demand and  $\zeta$ -potential, resulting in a higher density of binding sites. Moreover, the charged and entangled network of DA-TOCNFs allowed for the individualization of AgNPs, unlike DAC, where some agglomerations were observed. Overall, this study presents an improved single-step process for the synthesis of AgNPs on nanocellulose surfaces, highlighting their potential for safe and high-performance applications in food packaging. Paper sheets coated with nanocellulose/AgNPs suspensions fully inhibited the growth of *B. subtilis*, at least for one month after coating, and caused damage to their cell membranes. This research provides a one-pot facile route to fabricating hybrid nanocellulose/AgNPs systems, stable in water, and may be used directly as a coating layer for board and paper active packaging with little or even undetectable release of Ag.

**Supplementary Information** The online version contains supplementary material available at <https://doi.org/10.1007/s10570-024-05918-5>.

M. Aouay · S. Boufi  
Faculty of Science, LMSE, University of Sfax, BP 802,  
3018 Sfax, Tunisia

R. J. Aguado · G. Bayés · N. Fiol ·  
M. Delgado-Aguilar (✉)  
LEPAMAP-PRODIS Research Group, University  
of Girona, C/ Maria Aurèlia Capmany, 61, 17003 Girona,  
Spain  
e-mail: m.delgado@udg.edu

G. Bayés  
Noel Alimentària SAU, Pla de Begudà, 17857 Begudà,  
Spain

J.-L. Putaux  
Univ. Grenoble Alpes, CNRS, CERMAV,  
F-38000 Grenoble, France

**Keywords** Antibacterial · Dialdehyde cellulose · Nanocellulose · Packaging paper · Silver Nanoparticles · TEMPO-mediated oxidation

## Introduction

In the upcoming years, both the food and food packaging industries will have to face important challenges. Considering that several strategies worldwide are aligned with the reduction of plastic use, particularly those designed for a single use, most of the food packaging solutions available in the market will require a sustainable modification, conception or even substitution for non-plastic products. A clear example of this is the Directive (EU) 2019/904 of the European Parliament and the Council (of 5 June 2019), broadly known as the single-use plastic (SUP) directive (European Commission 2019). Among the different highlighted materials and products in the abovementioned directive, food containers are proposed to be reduced, in contraposition to straws or beverage stirrers, which are directly banned. This difference level of exigence is motivated by the existing technological gap between the existing non-plastic materials and the requirements during their shelf life. Further, the next generation of food packaging must comply with the existing food safety regulations (i.e., European Regulation EC 1935/2004). These materials must also satisfy the technical requirements in terms of resistance to liquids, barrier to gases and dimensional stability under different climatic and usage conditions, which may vary from one type of food to another.

Despite the negative environmental impacts of plastic-based packaging, particularly if not properly managed at its end of life, there is no doubt that the barrier performance of both mono- and multi-material plastic structures can offer is much greater than those based on paper (Kumar et al. 2016; Tyagi et al. 2019). This is the case of ethylene vinyl alcohol (EVOH), even combined with polyolefin, which exhibits excellent barrier properties to oxygen (Yeo et al. 2001). On the other hand, paper is a porous structure that needs to be properly modified to provide certain barrier to gases (Lavoine et al. 2012; Tarrés et al. 2018; Tyagi et al. 2019). Among these modifications, solutions based on nanocellulose, nanoclay, modified polysaccharide, or even natural wax coatings, have appeared as potential barrier solutions for paper structures (Hult et al. 2010; Khwaldia 2010; Rastogi and Samyn 2015). Indeed, the use of nanocellulose as paper additive is not new, and it has been widely studied for several purposes, being paper strengthening the most widely reported (Boufi et al. 2016; Brodin et al. 2014; González et al. 2012;

Hii et al. 2012). However, its use as paper coating is becoming a topic of great interest and several studies on this direction have appeared in the last years, using either pure nanocellulose, both cellulose nanofibrils (CNFs) and nanocrystals (CNCs), modified, or in combination with other coating agents to improve both surface and barrier properties (Hubbe et al. 2017; Lu et al. 2022; Mazega et al. 2022a; Tarrés et al. 2018; Tyagi et al. 2018).

The scientific community, being aware of the limitations of paper as plastic substitute for food packaging, has started to develop active materials that can contribute to food preservation. This includes inducing specific surface modifications to nanocellulose or blending with other materials for providing antioxidant or antimicrobial characteristics that could compensate the lower barrier performance of paper compared to mono and multilayer plastics (Anthierens et al. 2011; Fortunati et al. 2012, 2014; Mu et al. 2013). Among others, silver nanoparticles (AgNPs) have been extensively studied for their antimicrobial properties, having been reported to effectively inhibit the growth of both Gram-negative and Gram-positive bacteria (Busolo et al. 2010; Garza-Cervantes et al. 2020). Recently, their incorporation into paper-based substrates has become increasingly popular, standing as the most frequent antibacterial agent in the literature (Aguado et al. 2019; Jung et al. 2018). Most likely, considering the complexity of a paper production line, coating stages offer the best opportunity to add AgNPs onto the surface of paper or board. It comes as no surprise, then, that most projects on silver-containing paper opt for coating as the method of incorporation (Amini et al. 2016; Busolo et al. 2010). In any case, the resulting AgNPs-paper products can be useful in applications where hygiene is essential, such as food packaging and paper for hospitals (He et al. 2021). Indeed, the use of AgNPs is not limited to paper coating, as they are also present in biomedical products such as wound healing devices (Shalaby et al. 2015). Moreover, considering the difficulties to clean paper (unlike glass or steel, for instance), any paper-based material to be reused instead of disposed could benefit from the antimicrobial properties granted by AgNPs.

In most of the reports, the combination of AgNPs with CNFs is a two-stage process, where AgNPs are firstly produced by reducing silver salts (i.e.,  $\text{AgNO}_3$ ) and then incorporated into a CNF suspension. This

strategy usually encompasses the use of reducing agents whose industrial production implies boron mining, although several strategies have been reported for replacing them, such is the case of using lignocellulosic residues or citric and tannic acid (Bastos-Arrieta et al. 2018; La Spina et al. 2020). Other strategies may encompass the addition of the reducing agent to the metal precursor in the presence of CNFs. However, the combination of CNFs with other reducing agents leads to AgNPs formed in solution, and not immobilized onto the CNF surface (Wang et al. 2014). In some other cases, nanocelluloses have been used as both reducing agents and immobilizers, taking advantage of the reducing capacity of hydroxyl groups. However, the presence of other functional groups (i.e. carboxyl or aldehyde) can interfere with the nucleation process of AgNPs by means of coordination (Ifuku et al. 2009). Finally, the surface functionalization of the cellulose chain has been also proposed, providing to this substrate the capacity of both reducing the silver salt and immobilizing the resulting nanoparticles onto its surface (Errokh et al. 2019). For instance, dialdehyde cellulose (DAC) can be easily obtained by means of C2-C3 ring opening through periodate oxidation. DAC has been previously reported as an excellent both reducing and immobilizing agent for AgNPs production (Errokh et al. 2019; J. Li et al. 2018).

Despite the well-known aptitude of the aldehyde group to act as a reducing agent for silver through what is known as Tollens' reaction, only limited contributions have been focused on the preparation of hybrid nanocellulose/AgNPs. For instance, in 2019, dialdehyde cellulose nanocrystals (DACNCs) were used as both the reductant and stabilizer for the preparation of CNC-AgNPs composite. CNC-AgNPs was added into the pulp slurry to produce antibacterial paper (Xu et al. 2019). In another study, AgNP-decorated dialdehyde nanofibrillated cellulose (DATNFC@Ag) was prepared by the periodate oxidation of already prepared TEMPO-oxidized nanofibrillated cellulose followed by silver reduction. The film containing DATNFC@Ag exhibited antibacterial activity against both *Staphylococcus aureus* and *E. coli* (J. Li et al. 2019). In fact, the in-situ reduction approach offers the following advantages; (i) less consumption of chemicals, as no external reducing agent is added, (ii) less tendency of the aggregation of AgNPs, (iii) favor the binding of Ag on the surface of the fibrils, and (iv) lower size of the generated NPs.

Others have reported the AgNPs synthesis in carboxylated cellulose species. However, in most of the cases the presence of a reducing precursor for Ag ions is required, such is the case of sodium borohydride or ascorbic acid (Uddin et al. 2014; Pawcenis et al. 2019). Studies that did not report the use of additional reducing agents for one-pot AgNPs synthesis onto carboxylated cellulose, indicated that either a high-temperature treatment or UV irradiation for varying times were required (Hosseinioust et al. 2016; Zhang et al. 2019). While the previous work constitutes a significant advancement towards the development of nanocellulose-based AgNPs suspensions for several applications, the present work provides a one-pot preparation of AgNPs in cellulose through the symbiotic action between aldehyde and carboxylic groups, with no need of postprocessing of the samples.

The present work reports a one-pot preparation of DAC/AgNPs and DA-TOCNF/AgNPs hybrid nanofibrils by simply mixing at room temperature the DAC and TOCNFs suspension with  $(\text{Ag}(\text{NH}_3)_2\text{OH})$ . The hybrid nanocellulose/AgNPs suspension is then applied as an antimicrobial coating for packaging paper. The main emphasis is to give insight into how the functionality of the cellulose fibrils would control the amount of appended AgNPs, as well as their locus with respect to the surface of the nanocellulose fibrils. The merit of the hybridization of AgNPs with nanocellulose, in terms of the reduced risk of Ag release when nanocellulose/AgNPs is intended for food packaging, is also demonstrated. In addition, no intermediate step for the preparation of nanocellulose is required, as the present approach allows for the functionalization of the cellulose and for their break-down into nanocellulose via a mild disintegration treatment. All these aspects of the present work have not been reported in the literature so far and constitute a source of novelty in the field of hybrid nanocellulose/AgNPs.

## Experimental section

### Materials

Bleached kraft eucalyptus pulp (BKEP), in the form of never-dried laps, was kindly supplied by Torraspapel S.A. The selected brown-line paper was a testliner (TSL) kindly provided by SAICA (Zaragoza, Spain). Its basis weight was  $(170 \pm 1) \text{ g m}^{-2}$ .

Silver nitrate ( $\text{AgNO}_3$ ), nitric acid ( $\text{HNO}_3$ ), aqueous ammonia ( $\text{NH}_3$  25 wt%), sodium bromide ( $\text{NaBr}$ ), sodium hypochlorite ( $\text{NaClO}$ ), sodium hydroxide ( $\text{NaOH}$ ), hydroxylamine hydrochloride ( $[\text{NH}_2\text{OH}]^+\text{Cl}^-$ ), and sodium metaperiodate ( $\text{NaIO}_4$ ) were purchased from Scharlab SL (Sentmenat, Spain). (2,2,6,6-tetramethylpiperidin-1-yl)oxyl (TEMPO) and poly(vinyl alcohol) (PVA: hydrolysis degree of 86.7–88.7 mol%;  $M_w = 130 \text{ kg mol}^{-1}$ ) and were provided by Sigma-Aldrich Química SA (Barcelona, Spain). Sodium polyethylene sulfonate (PES-Na) and poly(diallyldimethylammonium chloride) (PDADMAC) were supplied by BTG Instruments GmbH (Weßling, Germany). All reagents were used as received with no further purification.

Non-pathogenic strains of *Escherichia coli* and *Bacillus subtilis* were received from the American Type Culture Collection (Manassas, VA, USA).

#### Production of modified celluloses and characterization

The never-dried BKEP laps (30 g on a dry basis) were disintegrated in a laboratory pulper operating at 3,000 rpm for 20 min at 1.5 wt% consistency. This process was repeated twice, as one batch was subjected to TEMPO-mediated oxidation and the remaining one was kept at 4 °C for further use. TEMPO-mediated oxidation took place at pH 10 and at a consistency of 1 wt%. Briefly, 3 g of NaBr and 480 mg of TEMPO were first dissolved in distilled water until complete dissolution. Then, 30 g of disintegrated BKEP (over dry weight) were incorporated into the digester and maintained under gentle stirring. Once the fiber was dispersed, 450 mmol of NaClO (i.e.,  $15 \text{ mmol g}^{-1}$ ) were added. A 0.5 M NaOH solution was used to adjust the pH. After the reaction, the oxidized pulp was thoroughly washed with distilled water and filtered. The oxidized pulp underwent high-pressure homogenization in a NS1001L PANDA 2 K from GEA (Parma, Italy), operating at 1 wt% consistency, at the sequence of 3 passes at 300 bar and 2 passes at 600 bar. The resulting TEMPO-oxidized cellulose nanofibrils (TOCNFs) were then stored in a hermetic plastic bag and kept at 4 °C for further use and characterization. The carboxyl content was used as a control parameter and determined according to a previously reported method (Serra et al. 2017). For comparison purposes, the procedure was repeated with a NaClO dosage of  $3 \text{ mmol g}^{-1}$ .

Both TOCNFs and the second batch from the laboratory pulper were subjected to a periodate oxidation treatment with  $\text{NaIO}_4$ . The reaction took place in a closed borosilicate glass container, held at 40 °C for 48 h with magnetic stirring, and protected from sunlight. The ratio, on a dry basis, of  $\text{NaIO}_4$  to cellulose was set at 1.2 and  $0.7 \text{ g g}^{-1}$  for BKEP and TOCNFs, respectively. The resulting suspensions were thoroughly washed by centrifugation ( $4000 \times g$ , 10 min) to remove the excess of  $\text{NaIO}_4$ . After the process, two different dialdehyde-modified cellulose derivatives were obtained, namely that directly obtained from BKEP (DAC) and that obtained from TOCNFs (DA-TOCNFs). Aldehyde content was estimated by hydroxylamine hydrochloride binding and subsequent titration with NaOH (Wei et al. 2016).

The original pulp (BKEP), TOCNFs, DAC and DA-TOCNFs were characterized in terms of cationic demand (CD), transmittance of the suspension and  $\zeta$ -potential. CD was estimated by potentiometric back titration, as reported elsewhere (Serra-Parareda et al. 2021). For that, 1 g of each suspension was suspended in 25 mL of PDADMAC 0.001 N, kept under gentle stirring for 10 min and centrifuged at  $4000 \times g$  for 10 additional minutes. Then, a 10-mL aliquot was taken from the supernatant, where excess of PDADMAC was expected, and introduced in a particle charge detector PCD-06 from BTG Instruments (Weßling, Germany). The equipment provided the potential of the suspension, which was then titrated with PES-Na until the isoelectric point (0 mV) was reached. The CD was then calculated according to Eq. 1.

$$CD = \frac{C_{p^+} \cdot V_{p^+} - C_{p^-} \cdot V_{p^-}}{w_{\text{sample}}} \quad (1)$$

where  $C_{p^+}$  is the original concentration of PDADMAC (0.001 N),  $C_{p^-}$  is the concentration of PES-Na,  $V_{p^+}$  and  $V_{p^-}$  are their respective volumes, and  $w_{\text{sample}}$  is the mass of sample on a dry basis.

Transmittance was determined at 600 nm of wavelength of 0.1 wt% suspensions in a Shimadzu UV-1201 spectrophotometer (Shimadzu Europa GmbH, Duisburg, Germany), using distilled water as reference. A particle size analyzer from Malvern Panalytical (Malvern, United Kingdom) was used to record the  $\zeta$ -potential of 0.05 wt% suspensions, at pH

6.5–7.5 and using Malvern's folded capillary cell with gold electrodes.

Drops of dilute suspensions were deposited onto carbon-coated grids for transmission electron microscopy (TEM). The excess liquid was blotted with filter paper and a drop of uranyl acetate negative stain was deposited before complete drying. The excess stain was blotted, and the grid allowed to air-dry. The preparations were observed using a JEOL JEM-2100 Plus microscope (JEOL Ltd, Japan) operating at 200 kV and images were recorded with a Rio 16 camera (Gatan, United States).

#### In-situ AgNPs synthesis and characterization of the suspensions

The Tollens' reagent in its alkaline form,  $\text{Ag}(\text{NH}_3)_2\text{OH}$ , was obtained by mixing equimolar amounts of  $\text{AgNO}_3$  (0.1 M) and  $\text{NaOH}$  (0.1 M), and the resulting  $\text{Ag}_2\text{O}$  was dissolved in excess aqueous ammonia. To 1 g of DAC or DA-TOCNFs (on a dry basis), enough  $\text{Ag}(\text{NH}_3)_2\text{OH}$  was added so that the concentration of the latter was  $5 \cdot 10^{-3}$  M,  $10^{-2}$  M,  $5 \cdot 10^{-2}$  M, or  $10^{-1}$  M, depending on the case. The pH of the suspension after mixing  $\text{Ag}(\text{NH}_3)_2\text{OH}$  with nanocellulose was around 6.5–7 for all samples, irrespective of the  $\text{Ag}(\text{NH}_3)_2\text{OH}$  concentration. Trials over the TOCNFs were also performed, as revealed by the video provided as Supporting Information (Video S1).

Mixtures were centrifuged at  $4000 \times g$  for 40 min in a Macrotronic-BLT centrifuge from JP Selecta (Abrera, Spain) several times, removing the supernatant in each case and adding distilled water to remove the excess of non-reduced silver, even if it implied the loss of some DAC/AgNPs or TOCNF/AgNPs. Finally, the stable and concentrated sediment was kept at 4 °C for further use and characterization.

AgNP-containing suspensions were characterized in the same terms than those described for BKEP, TOCNFs, DAC, and DA-TOCNFs. However, suspensions containing AgNPs were also subjected to surface plasmon resonance. The absorbance of the suspensions was determined in a Shimadzu UV-1201 spectrophotometer within the 350–750 nm range. The surface plasmon resonance of AgNPs was found to be at 420 nm, as it has been widely reported (Smitha et al. 2008).

#### Particle size and $\zeta$ -potential measurement

The particle size distribution and  $\zeta$ -potential measurements were measured by dynamic light scattering (Zetasizer Nano S, Malvern Instruments Ltd., Malvern, UK). The particle size was expressed as a Z-average size of an equivalent hard sphere with the same diffusion coefficient as the particle under analysis. The  $\zeta$ -potential was measured by laser doppler electrophoresis apparatus (NanoZetasizer ZS, Malvern Instruments Ltd., Malvern, UK). For each sample, the measurement was done in triplicate and the average value was taken as the particle size.

#### Film preparation and characterization

Films were prepared from the suspensions by solvent evaporation, on polystyrene Petri dishes held at 23 °C for 72 h. For that, suspensions containing *ca.* 0.4 g of DAC, DAC/AgNPs, DA-TOCNFs, and DA-TOCNFs/AgNPs (on a dry weight basis) were spread over the surface of the dishes (8 cm in diameter). The thickness of the resulting films was roughly 50  $\mu\text{m}$ . They were used for X-ray diffractometry (XRD), Fourier-transform infrared spectroscopy (FTIR), and inductively coupled plasma optical emission spectrometry (ICP-OES).

The films were probed in transmission mode by a Ni-filtered  $\text{CuK}\alpha$  X-ray beam ( $\lambda = 0.15142$  nm) produced by a Philips PW3630 generator operating at 30 kV and 20 mA (Philips, Suresnes, France). Two-dimensional diffraction patterns were recorded on Fujifilm imaging plates and read off-line with a Fujifilm BAS 1800-II bioanalyzer (Fujifilm Europe GmbH, Duesseldorf, Germany). Diffraction profiles were calculated by radially averaging the 2D patterns. Baseline subtraction was performed with the Origin-Pro software package (OriginLab), creating the zero counts line with the 2nd derivative method. Peaks were deconvoluted and the full width at half-maximum (FWHM) was read in the horizontal axis ( $2\theta$ ). The average crystallite size was estimated with Scherrer's equation (Eq. 2):

$$D = \frac{k \cdot \lambda}{FWHM \cdot \cos\theta} \quad (2)$$

In Eq. 2, the shape factor  $k$  can be assumed as 0.90 for silver (Shaaban et al. 2021). FWHM is expressed in radians, and  $\theta$  is Bragg's angle.

These films were also analyzed by FTIR using a Bruker Alpha II FTIR spectrometer (Bruker, Madrid, Spain), equipped with an ATR apparatus and operated with the OPUS software. The resolution was  $4\text{ cm}^{-1}$ .

For quantitative analysis, samples were digested in concentrated nitric acid and submitted to ICP-OES, performed in an Agilent 5100 device from Agilent Technologies (Santa Clara, CA, USA), to determine their total Ag content. Moreover, the thermal degradation behavior of each film was assessed by means of a TGA/DSC1 device from Mettler-Toledo (Cornellà de Llobregat, Spain). For that, samples were heated at a rate of  $10\text{ K min}^{-1}$  from  $25\text{ }^{\circ}\text{C}$  to  $800\text{ }^{\circ}\text{C}$ , under oxidizing atmosphere (air).

#### Paper coating and characterization

The coating process of the developed AgNP-rich suspensions was performed over commercial grade TSL papers to assure uniformity and regularity between samples. For this, the solid content of the suspensions was adjusted to 3 wt% and bar-coated using a K Control Coater from RK Print Coat Instruments LTD (Litlington, United Kingdom) using the smooth roll (number 0). The size of the paper sheets was the equivalent to an A4 ( $297 \times 210\text{ mm}^2$ ) and the coating speed was set at  $5\text{ m}\cdot\text{min}^{-1}$ . The volume of the suspension was set at 4 mL, which ensured the full coverage of the paper sheet. The excess of water was removed by means of air drying, and complete drying was achieved in a vacuum drier from a Rapid-Köthen sheet former, setting the suction pressure at 96 kPa and according to ISO 5269-2:2004.

In order to assess the total migration of silver to the foodstuffs, paper samples were cut into 4 cm squares and immersed in 100 mL of two different food simulants for 24 h: ethanol/water mixture (50 vol%), also known as simulant D1, and a 3 wt/vol% acetic acid, known as simulant B. The total Ag content of the extract was quantified by ICP-OES after acidifying with nitric acid.

Papers were also observed by optical microscopy by means of a DMR-XA microscope from Leica (Wetzlar, Germany), using halogen illumination. In addition, the surface of paper samples was sputter-coated with carbon and observed in secondary electron mode using a ZEISS DSM 960A (ZEISS Iberia, Madrid, Spain) field-emission scanning electron microscope (FE-SEM) operating at a 7 kV.

#### Proof of concept: double-side coated paper

Finding that paper sheets coated with either DA-TOCNFs/AgNPs or DAC/AgNPs did not have appropriate gas barrier properties to be used for food packaging, a double-side coating strategy was proposed with the aim of producing a successful proof of concept for this application. Hence, one side was coated with DA-TOCNFs/AgNPs (as they were found to outperform DAC/AgNPs), following a preparation process with Tollens' reagent ( $10^{-2}\text{ M}$ ). This side is intended to be in contact with the foodstuff and is meant to attain antimicrobial activity. The other side (*i.e.*, the air side) was coated with a 2 wt% PVA solution at  $50\text{ }^{\circ}\text{C}$ .

The air resistance of paper (Gurley method) was addressed following the TAPPI test method T460. The water vapor transmission rate (WVTR) was quantified by the dry cup method (ASTM 2017). Briefly, paper samples were placed on impermeable cups containing silica gel. The cups were sealed, kept in a conditioned chamber at  $23\text{ }^{\circ}\text{C}$  and 50% of relative humidity, and regularly weighted to compute the increase in mass due to permeated water vapor.

Regarding key mechanical properties, the burst index of uncoated and coated paper was measured with a device from IDM (Donostia-San Sebastián, Spain) that complies to the ISO standard 2759. The tensile properties (ISO 1924-2) and the tear index were determined by a universal testing machine (Instron, Barcelona, Spain) and by an Elmendorf tester (IDM), respectively (ISO 2011).

The activity against the Gram-positive bacteria *Bacillus subtilis* and against the Gram-negative bacteria *Escherichia coli* was tested by a variation of the disk diffusion method (noting that diffusion was not intended). First,  $100\text{ }\mu\text{L}$  of a bacterial culture in each case (*ca.*  $10^6\text{ CFU}$ ) were spread over sterilized Mueller–Hinton agar, in polystyrene Petri dishes (diameter: 80 mm). Then, coated paper disks (diameter: 25 mm) were placed over the inoculated medium. Dishes were sealed with Parafilm (Neenah, WI, USA) and incubated at  $37\text{ }^{\circ}\text{C}$  for 48 h. The antibacterial activity was assessed in qualitative terms, *i.e.*, whether there was growth over the surface of paper disks. Then, other identical coated papers were aged at  $23\text{ }^{\circ}\text{C}$  and a relative humidity (RH) of 50%, exposed to air for 15 days and 30 days. The antibacterial activity of

these aged papers was assessed again, placing them on inoculated Petri dishes and submitting them to an incubation period of 48 h. Tests were performed in duplicate.

## Results and discussion

### Key properties of the coating suspensions

Periodate oxidation of BEKP resulted in 1.25 mmol –CHO per gram of DAC (Table S1), with a reaction yield of 65%. The rest of the cellulose was solubilized in the supernatant and thus discarded along the consecutive centrifugations. In all cases, when a slurry of DAC or DA-TOCNFs was mixed with the Tollens' reagent ( $[\text{Ag}(\text{NH}_3)_2]^+$ ) at room temperature, the suspension absorbed progressively more visible light, as  $\text{Ag}^+$  was reduced to AgNPs. The strong darkening, even at very low concentrations (see Video S1), is due to the oscillation of electrons on the surface of the nanoparticles, a phenomenon widely known as surface plasmon resonance (Karami and Taher 2018; Lou et al. 2011). It is worth mentioning that the color change from transparent to brownish occurred immediately as the  $[\text{Ag}(\text{NH}_3)_2]^+$  reagent was added (Video S1), with a deeper color observed in the presence of DA-TOCNFs. As the color of the suspension originates from the plasmon of AgNPs, this indicated that the whole process involving the reduction, nucleation and formation of AgNPs took place readily and rapidly, without the need to increase the temperature, nor add any external reducing agent. The absorption peaks are broad, but their maxima can be distinguished at roughly 416 nm (Fig. 1). The significant broadening of the plasmon resonance peak for the sample with the highest amount of Tollens' reagent likely results from the heterogenous distribution in the particle size of AgNPs, and from the morphology of these nanoparticles (Link and El-Sayed 1999).

Figure 1 reveals remarkable differences between DAC and DA-TOCNFs for equal concentrations of silver precursor. This could be also directly observed on the suspensions, where DA-TOCNFs with a  $[\text{Ag}^+]$  of  $10^{-2}$  M (Fig. 1c) exhibited a much more intense and darker color than in the case of DAC at the same  $[\text{Ag}^+]$  (Fig. 1b). The higher absorbance of the latter is suggestive of a higher concentration of silver,

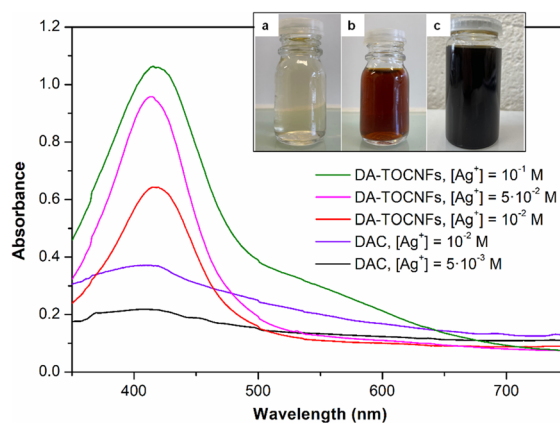


**Fig. 1** Visible absorption spectra of the suspensions of DAC and DA-TOCNFs with AgNPs. The total solids content was 0.005 wt%, except for  $[\text{Ag}^+] = 5 \cdot 10^{-2}$  M and  $[\text{Ag}^+] = 10^{-1}$  M, for which it was 0.002 wt%. Inset image: photographs of DAC (a), DAC with AgNPs- $10^{-2}$  M (b), and DA-TOCNFs with AgNPs- $10^{-2}$  M (c). These suspensions had been freshly prepared at the time of the picture

meaning that the generation of AgNPs was favored when both aldehyde and carboxylic groups were present. Moreover, there were hyperchromic shifts as the concentration of silver precursor went up, which also implies an increasing number of AgNPs. More details concerning the properties of the prepared samples are given in Table S1.

With a cationic demand of roughly  $0.7 \text{ meq g}^{-1}$  (Table 1), DA-TOCNFs nanofibrils presented both aldehyde groups to grant the reduction of the Tollens' reagent (Zeng et al. 2023) and, not less importantly, charged groups to attain electrostatic repulsion from each other. Indeed, for a silver ion concentration of  $10^{-2}$  M, DA-TOCNFs attained a highly negative  $\zeta$ -potential,  $-32 \text{ mV}$  (Table 1). Electrostatic repulsion is also linked to higher surface area and, thus, for a similar degree of substitution, more aldehyde groups were exposed to the Tollens' reagent in the case of DA-TOCNFs (Serra-Parareda et al. 2021). Although isolated AgNPs in aqueous media generally possess negative  $\zeta$ -potential (Elamawi et al. 2018), their association with TOCNFs led to certain neutralization of the electric double layer. Both the cationic demand and the  $\zeta$ -potential decreased when increasing the concentration of Ag precursor.

The CD experienced an unexpected tendency, particularly comparing the TOCNFs with the DA-TOCNFs

**Table 1** Some key electrokinetic and optical properties of the suspensions of cellulose, cellulose derivatives, and the combinations of them with Tollens' reagent. Tolerance intervals comprise twice the standard deviation

	[Ag <sup>+</sup> ] (mol L <sup>-1</sup> )	Cationic demand (μeq g <sup>-1</sup> )	Transmittance at 600 nm (%)	ζ-potential (mV)
BKEP	0	33 ± 3	–	–
DAC	0	182 ± 11	14.6 ± 0.3	-6 ± 1
	10 <sup>-2</sup>	186 ± 5	8.5 ± 0.4	-16 ± 2
TOCNFs	0	1740 ± 110	90.2 ± 1.0	-28 ± 1
	10 <sup>-2</sup>	1031 ± 29	19.0 ± 0.4	-32 ± 2
DA-TOCNFs	0	713 ± 20	65.8 ± 0.6	-33 ± 2
	10 <sup>-2</sup>	658 ± 36	37.0 ± 1.9	-24 ± 1
	5 · 10 <sup>-2</sup>	542 ± 16	0.0	-13 ± 1

in the absence of AgNPs. The CD of the TOCNFs accounted for 1740 μeq g<sup>-1</sup>, which is consistent with previous reports (Tarrés et al. 2017). However, when these TOCNFs were subjected to NaIO<sub>4</sub> oxidation, the CD experienced a significant decrease, roughly 60%, while in the case of BKEP, the CD increased from 33 to 273 μeq g<sup>-1</sup> due to this oxidation. While this contrasting behavior was observed, the trend with the incorporation of AgNPs was the same for DAC as for DA-TOCNFs. The lower CD of DA-TOCNFs compared to TOCNFs is hypothesized to be attributed to the unsuitability of the potentiometric back titration method for CD determination in the case of DA-TOCNFs. This method is based on determining the excess of PDADMAC (non-adsorbed) after a certain contact time. In this regard, the sample undergoes intense centrifugation, assuming that this excess is present in the supernatant. However, this method is suitable for non-soluble samples, while during the oxidation process with NaIO<sub>4</sub>, some cellulose fibers (TOCNFs, in this case) dissolve. As a result, the sample taken from the supernatant may contain both excess PDADMAC and a portion of the solubilized fraction of DAC (or DA-TOCNFs) neutralized by PDADMAC. Indeed, the decrease in the ζ-potential (increase in absolute terms) evidenced that DA-TOCNFs were more anionic than TOCNFs, supporting the hypothesis of the unsuitability of the potentiometric back titration for determining the CD in this type of sample.

The FTIR spectra recorded for these suspensions, once water was evaporated, are displayed in Fig. 2. The most relevant bands in what pertains to the molecular and supramolecular structure of cellulose, along with the bands assigned to vibrations of the key functional groups to reduce and/or bind AgNPs, are highlighted (Cael et al. 1974; Xu et al. 2019). The

broad band at 3328 cm<sup>-1</sup> corresponds to the stretching of hydrogen-bonded O–H, for which a significant loss of absorption was found for DAC and DA-TOCNF samples. The loss of supramolecular order is confirmed by the difficulty in distinguishing any peak at 1430 cm<sup>-1</sup>, characteristic of crystalline cellulose I. Indeed, the ratio of the intensity at this band and that at 890 cm<sup>-1</sup> has often been used to estimate the crystallinity index (Kljun et al. 2011) but, given the different empirical formulas of DAC derivatives, this work cautiously opts for leaving the change in intra- and intermolecular forces as a qualitative remark. Similarly, to the band at 890 cm<sup>-1</sup>, the prominent peak at 1024 cm<sup>-1</sup>, assigned to C–O–C ether bonds in the

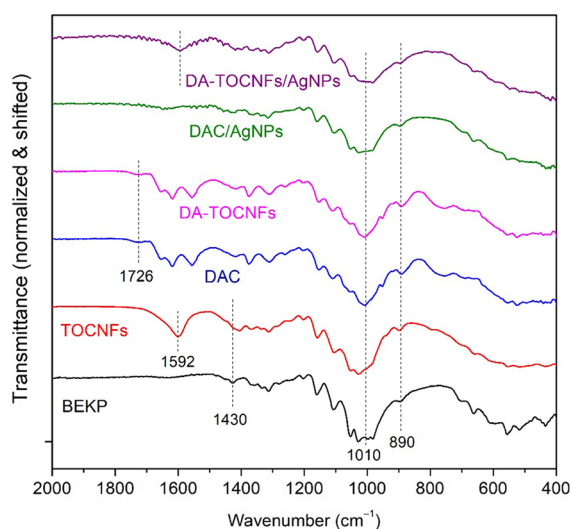


**Fig. 2** FTIR spectra of the starting cellulosic material (BKEP), films of its oxidized derivatives, and the combinations of the latter with the silver precursor ([Ag<sup>+</sup>] = 10<sup>-2</sup> M)

anhydroglucose ring, is also common to all samples (Aguado et al. 2021; Cael et al. 1974).

Regarding the groups resulting from the two different oxidations of hydroxyl groups, both carbonyl (DAC, DA-TOCNFs) and carboxylate groups (TOCNFs, DA-TOCNFs) are manifested by the asymmetric stretching vibration of C=O bonds. They correspond to bands at  $1726\text{ cm}^{-1}$  (weak) and  $1592\text{ cm}^{-1}$  (medium), respectively (Chung et al. 2004; Kolya et al. 2022). It can be argued the incorporation of AgNPs with a certain concentration of Tollens' reagent ( $10^{-2}\text{ M}$ ) exerted a hypochromic effect on both bands, especially in the one assigned to aldehyde groups. This may confirm the binding interaction, even after reduction of  $\text{Ag}^+$ , between oxidized functional groups and AgNPs.

The analysis of the colloidal properties of DAC and DA-TOCNFs prior to and after the addition of  $\text{Ag}(\text{NH}_3)_2\text{OH}$  was made to check whether the formation of AgNPs would alter the dispersion state of the nanocellulose suspension. Even though the DLS measurement is expressed in terms of the diameter of an equivalent hard sphere with the same diffusion coefficient as the particle under analysis, the method is useful to discern any aggregation effect. From Fig. 3a, it can be seen that the addition of  $\text{Ag}(\text{NH}_3)_2\text{OH}$  led to an upward shift of the particle size distribution, with an increase in the Z-average mean size from 280 nm for DAC to about 700 nm for DAC/AgNPs, and from 520 nm to about 820 nm for DA-TOCNFs/AgNPs. The  $\zeta$ -potential became more negative for DA-TOCNFs/AgNPs ( $-31\text{ mV}$ ) than for DAC/AgNPs ( $-16\text{ mV}$ ), owing to the nominal negative charge of carboxylate groups and to the conversion of aldehyde groups into carboxylate groups.

#### Morphological aspects of nanocellulose derivatives and AgNPs

The morphological differences between the various fractions of nanocellulose were characterized by TEM. TOCNFs are well-individualized slender nanofibrils containing kinks and entangled into networks (Fig. S1). DAC particles are much shorter and their morphology is more typical of CNCs constituted of a few laterally associated crystallites that were not separated by the treatment (Fig. 4a). DA-TOCNFs retain characteristics of both fractions: long individual nanofibrils can be seen as

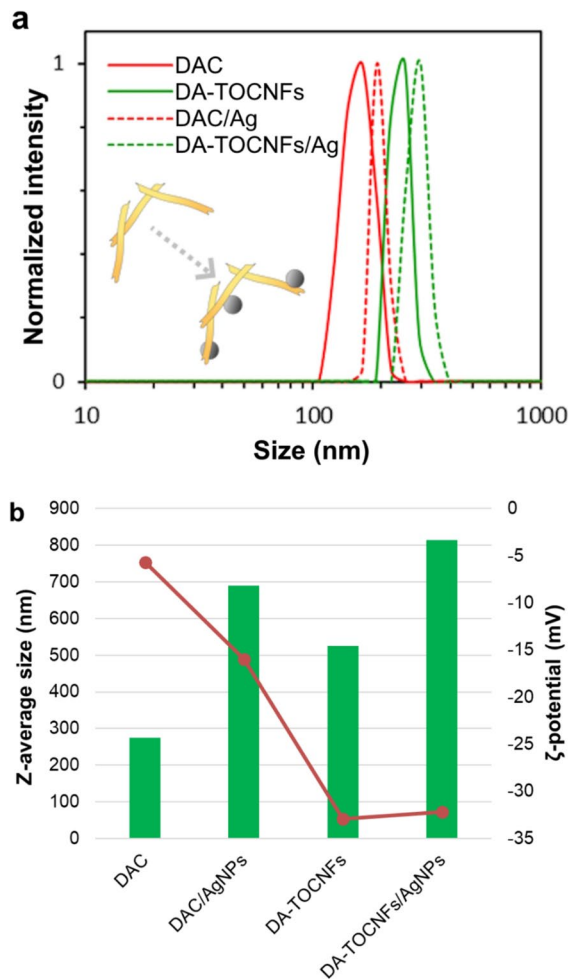
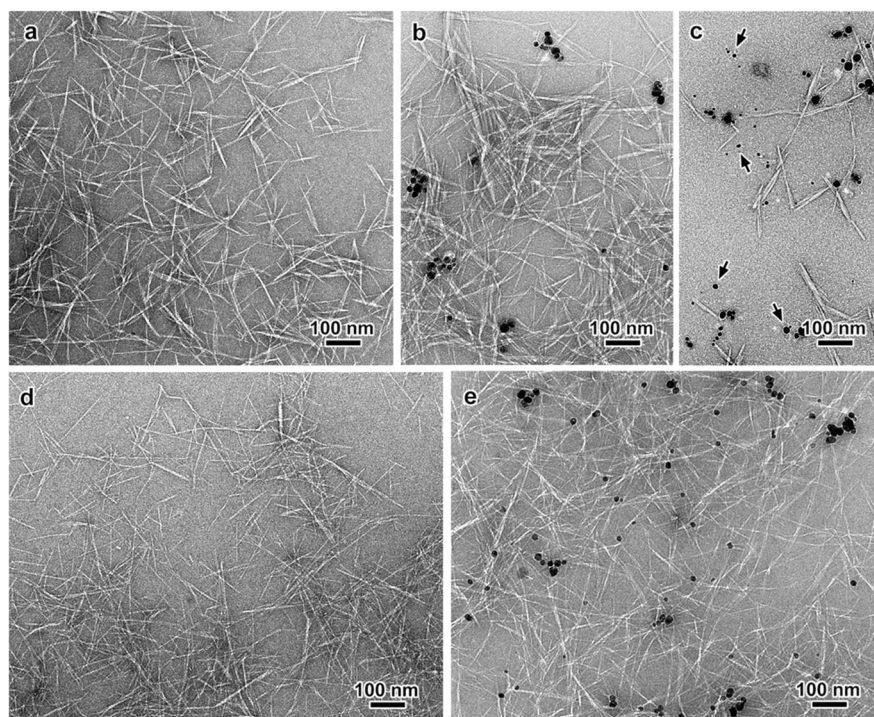


**Fig. 3** Particle size distribution of DAC and DA-TOCNF before and after the formation of AgNPs (a), and Z-average mean size of the corresponding suspension at pH 6.5–7 (b)

well are shorter segments thinner than the DAC particles (Fig. 4d).

XRD profiles were recorded with the X-ray beam perpendicular to the nanocellulose films (Fig. 5a). The typical peaks of native cellulose I can be recognized: overlapping 110 and  $1\bar{1}0$ , 200 and 004 (French 2014). However, the relative intensities of these peaks significantly vary when compared to those of untreated cellulose. XRD profiles were thus recorded with the beam parallel to the films ( $//$ ). As seen in Fig. 5b, the relative intensities in the profiles recorded in both film orientations are different. This effect has already been documented in the literature (Brito et al. 2012; Elazzouzi-Hafraoui et al. 2008)

**Fig. 4** TEM micrographs of negatively stained preparations from DAC (a–c) and DA-TOCNFs (d, e) suspensions before (a, d) and after (b, c, e) formation of AgNPs- $5 \times 10^{-2}$  M). The arrows in (c) point to AgNPs that are not immobilized onto the cellulose surface



and is due to preferential orientations of nanocellulose particles upon drying into a film, rather than specific degradations of the crystals during the oxidation treatments. This uniplanarity effect seems to be stronger for DAC, which is consistent with the smaller size of the nanoparticles (Fig. 4a) that results in a higher degree of freedom to preferentially orient upon drying.

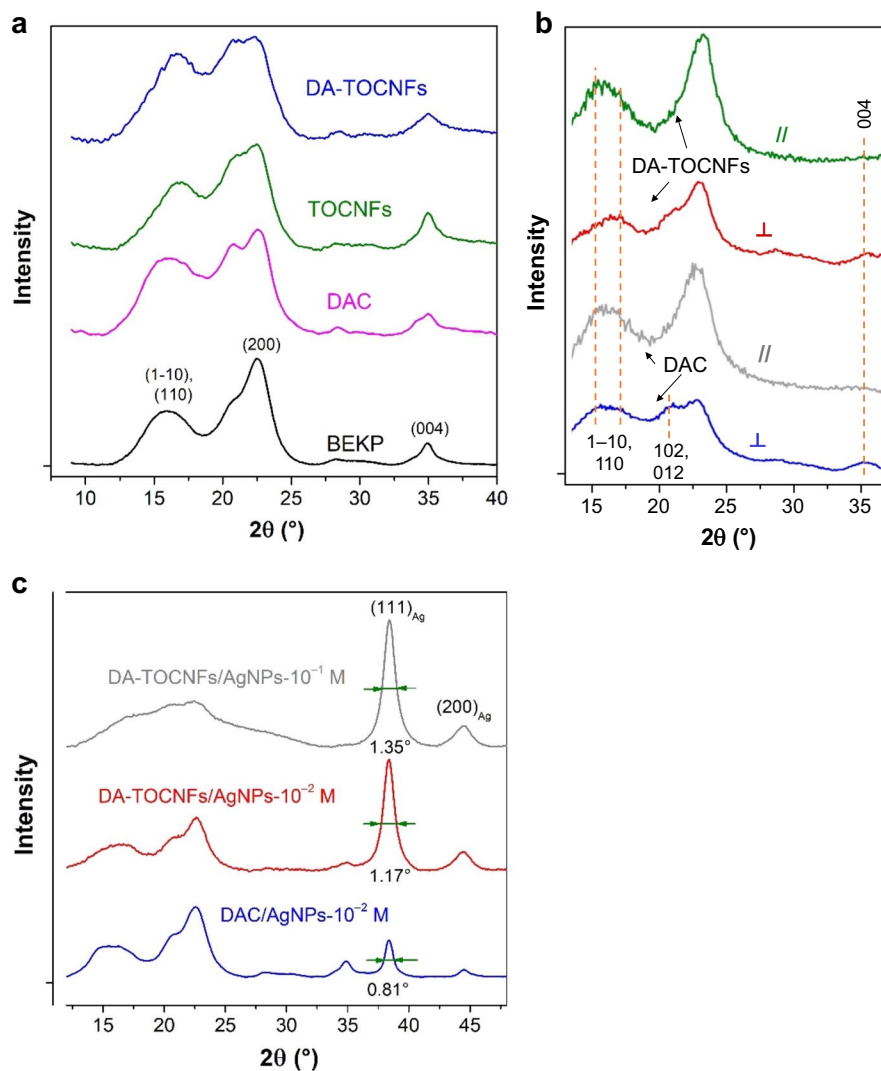
The impact of uniplanarity could also be seen in the XRD profiles of the samples treated with Tollens' reagent (Fig. 5c). The FWHM was calculated at the 111 peak of silver, along with the crystallite size as estimated therefrom (Table 2).

While the addition of Tollens' reagent in the TOCNFs suspension did not induce the formation of Ag, the AgNPs were formed on DAC (Fig. 4b) and on DA-TOCNF (Fig. 4e) seemed to be attached to the cellulose derivatives. These AgNPs exhibited different morphology, particularly in terms of size rather than in shape. This may be attributed to the presence of a large number of carboxyl groups in the later, since Tollens' reagent is in the form of  $[\text{Ag}(\text{NH}_3)_2]^+$  and may be attracted by the negative charges of  $\text{COO}^-$  groups. However, at the same time, the high surface area and the presence of a large number of

$\text{COO}^-$  groups kept the suspension stable (Fig. 3b). Moreover, the electrostatic interactions between carboxyl groups and Tollens' reagent could contribute to retaining the AgNPs at the surface of the fibrils, which was not the case for DAC (Fig. 4c). After the reduction process, isolated AgNPs were seen in DAC/AgNPs (Fig. 4c) but not in DA-TOCNFs, supporting the hypothesis that the ring-opening of cellulose in the form of a dialdehyde structure properly reduced  $\text{Ag}^+$  and immobilized the resulting AgNPs. In other words, while it is assumed that all reductions of  $\text{Ag}^+$  were mediated by adsorption regardless of the functionalization, desorption from DA-TOCNFs was more hindered than desorption from DAC. Regardless of the cellulosic derivative (DAC or DA-TOCNFs), both individual AgNPs and AgNP clusters could be appreciated. Nonetheless, this clustering could have been promoted by the removal of solvent and offers little information regarding the stability of DA-TOCNFs/AgNPs in aqueous media.

While TEMPO-mediated oxidation and  $\text{NaIO}_4$  oxidation affected the supramolecular structure of cellulose, a quantitative assessment of crystallinity was avoided out of caution. For instance, the use of one of the simplest methods, Segal's peak height method, is

**Fig. 5** X-ray diffraction profiles of cellulose derivatives (**a, b**) and their combinations with AgNPs (**c**). The profiles displayed to show the effect of the orientation of the incident beam on the sample (**b**) have not undergone background subtraction. Miller indices correspond to the stronger peaks of cellulose I $\beta$  and silver



arguable, as the selected cellulose derivatives exhibit different chemical structure. In addition, Segal's

**Table 2** Estimation of the crystallite size of AgNPs from XRD profiles

Crystallite	FWHM (°)	Size (nm)
AgNPs in DAC, $[Ag^+] = 5 \cdot 10^{-3}$ M	0.92	9.2
AgNPs in DAC, $[Ag^+] = 10^{-2}$ M	0.81	10.4
AgNPs in DA-TOCNFs, $[Ag^+] = 10^{-2}$ M	1.17	7.2
AgNPs in DA-TOCNFs, $[Ag^+] = 5 \cdot 10^{-2}$ M	1.30	6.5
AgNPs in DA-TOCNFs, $[Ag^+] = 10^{-1}$ M	1.35	6.2

method has been previously called into question, particularly for interpreting that the intensity between peaks results from peak overlap (French 2020; French and Santiago Cintrón, 2013; Segal et al. 1959).

Interestingly, the crystallite size of AgNPs was lower when Tollens' reagent was incorporated into DA-TOCNFs than in the case of DAC (Fig. 5c, Table 2). This may be attributed to the higher surface area of TOCNFs compared to the raw BKEP and, thus, of the DA-TOCNFs compared to DAC (Guo and Catchmark 2012; Agarwal et al. 2017). The higher availability of aldehyde groups in DA-TOCNFs compared to DAC probably resulted in an increasing number of reducing sites and, in addition, immobilization of smaller AgNP crystals.

### Extent of Ag<sup>+</sup> reduction

As evidenced by the results of ICP-OES assays, displayed in Fig. 6, DA-TOCNFs did not only reduce the silver precursor to a greater extent than DAC, but they also did so with direct proportionality to the concentration of Tollens' reagent. Pearson's coefficient correlating [Ag<sup>+</sup>] to the final proportion of Ag in the DA-TOCNFs/AgNPs systems was  $r=0.9991$ . Although this linearity should be taken with caution since it implies only three points, it is indicative of a chemical equilibrium shifted to the consumption of the limiting reagent (Ag<sup>+</sup>). This means that the presence of carboxylic groups in addition of the aldehyde functions boosts the generation of AgNPs in periodate-oxidized cellulose fibrils. To corroborate this conjecture, it can be indicated that DA-TOCNFs prepared with 3 mmol NaClO per gram of BEKP, resulting in a lower carboxyl content, reduced Ag<sup>+</sup> to a lesser extent (Table S1).

Beyond acting as a reducing agent for [Ag(NH<sub>3</sub>)<sub>2</sub>]<sup>+</sup> species, the cellulose nanofibrils would prevent the aggregation of AgNPs, resulting in the formation of a colloiddally stable suspension of modified cellulose/AgNPs. In fact, without the use of capping agents, or supports, metal NPs are known to be thermodynamically unstable and tend to aggregate during their bottom-up synthesis from ionic or molecular precursors. However, how one could explain the reduction of [Ag(NH<sub>3</sub>)<sub>2</sub>]<sup>+</sup> ions and the rapid growth of AgNPs selectively on the cellulosic substrate without the addition of an extra reducing and capping agent to stabilize AgNPs? The following mechanism is proposed to account for the particular morphology of DAC/AgNPs

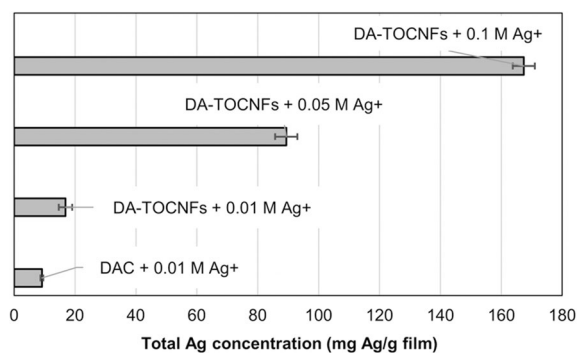


**Fig. 6** Concentration of total silver, regardless of the oxidation degree, in oxycellulose/AgNP systems (on a dry weight basis), according to ICP-OES

and DA-TOCNFs/AgNPs: The first step is the adsorption of Ag<sup>+</sup> ions on the surface of the cellulosic derivatives, via coordination with hydroxyl groups and electrostatic interactions with carboxylic groups. Secondly, each chelated [Ag(NH<sub>3</sub>)<sub>2</sub>]<sup>+</sup> ion is readily reduced by one aldehyde group into one Ag<sup>0</sup> atom according to Tollens' reaction, giving rise to two Ag<sup>0</sup>. The generated Ag<sup>0</sup> atoms along one nanofibril coalesce thanks to their close proximity, leading to the *in-situ* growth of AgNPs. Like in Tollens' reaction, the reduced Ag remained in contact with the aldehyde that is converted into a carboxylic group, the generated AgNPs are located essentially on the nanofibril, and further growth and aggregation of the AgNPs is restricted by steric hindrance, chelation, and electrostatic interaction of the NPs with the cellulosic derivatives. In this way, we expect that nanofibrils will contain only a limited number of AgNPs, as confirmed by TEM observations. Accordingly, modified cellulose nanofibrils not only provoke the effective bio-reduction of silver ions to AgNPs but also act as a support and capping agent to prevent AgNPs from agglomeration. The larger number of AgNPs when DA-TOCNFs were used could be explained by the presence of carboxylic groups on the nanofibrils that further enhance the adsorption of [Ag(NH<sub>3</sub>)<sub>2</sub>]<sup>+</sup> species on the CNFs. This tentative mechanism is illustrated in Fig. 7.

Regarding TGA analyses, results were qualitatively similar to those of Mehdaoui et al. (2021), showing that the thermal degradation of DAC can take place in up to three stages. From the thermograms in Fig. 8, it can be seen that the first onset of thermal degradation ( $T_{on}$ ) for DAC is much lower than that of DAC/AgNPs, which is presumably due to the fact that the aldehyde groups on DAC decreased its thermal stability (Varma and Chavan 1995). The shift to higher temperature for DAC/AgNPs is indicative of the consumption of the aldehyde group during the reduction process. Furthermore, the ash content in DAC/AgNPs (12%) is only slightly higher than that of DAC (3.5%), which may be due to the relatively low Ag content in DAC/AgNPs. Regarding the TGA curve of DA-TOCNFs, similarly to DAC, an upward shift of  $T_{on}$  to higher temperature could be seen, but the residue at 800 °C is much higher for DA-TOCNF/AgNPs (around 32%, against 12% for DA-TOCNFs). This further corroborates the higher amount of reduced Ag in DA-TOCNFs in comparison with DAC for the same Tollens' reagent concentration.

**Fig. 7** Schematic illustration of the formation and growth of AgNPs on DAC and DA-TOCNFs

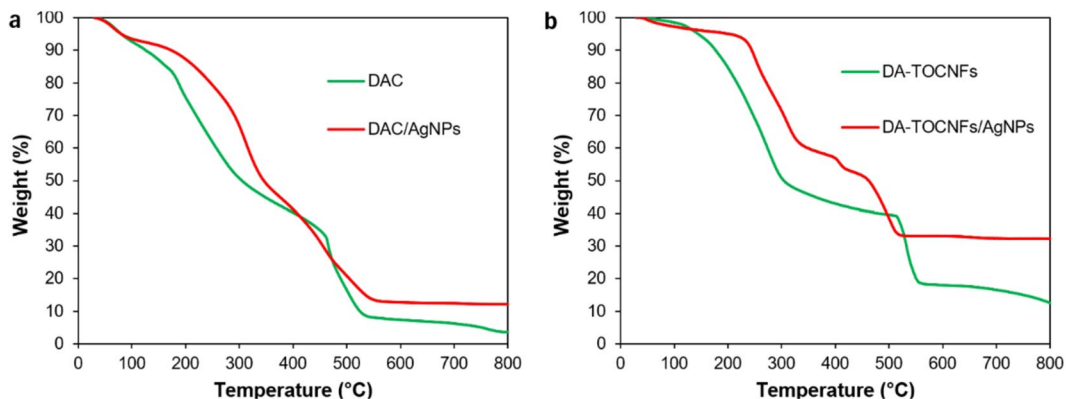
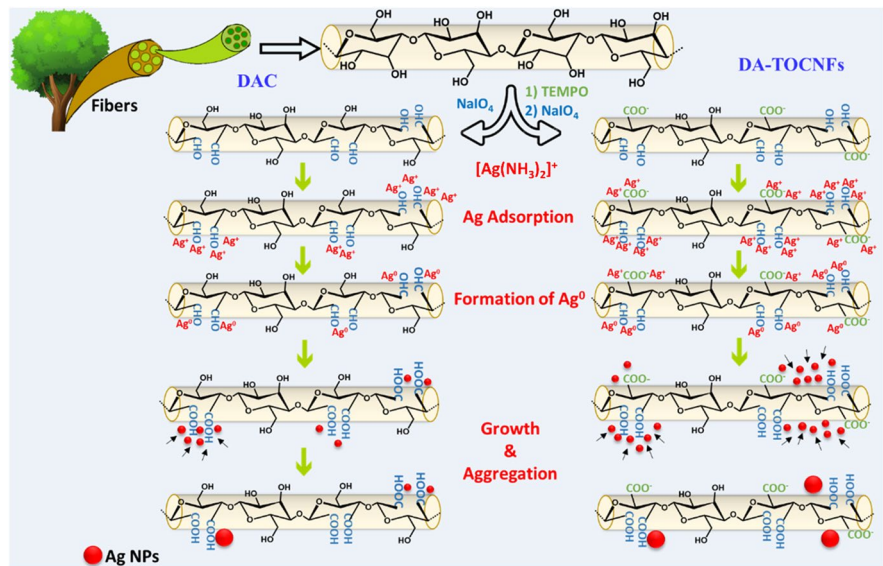


**Fig. 8** Thermal degradation behavior of DAC, DAC/AgNPs (a), and DA-TOCNF, DA-TOCNFs/AgNPs, (b)

DA-TOCNFs/AgNPs-coated paper: properties as passive material

The properties of the sheets coated with DA-TOCNFs/AgNPs (food contact side) and PVA (air side) are displayed in Table 3. Out of the  $(5 \pm 1) \text{ g m}^{-2}$  of coat weight, it can be estimated that  $(2 \pm 1) \text{ g m}^{-2}$  corresponded to DA-TOCNFs/AgNPs, since that was the basis weight gain of paper sheets coated with them, but without the PVA layer.

With DA-TOCNFs/AgNPs as the sole coating layer, paper sheets displayed insufficient gas barrier properties to be used for food contact. For instance, their air resistance increased only from  $29 \pm 1 \text{ s/100 mL}$  (uncoated)

to  $38 \pm 8 \text{ s/100 mL}$  (coated with DA-TOCNFs/AgNPs). This is why the sheets proposed for food packaging applications were coated with a partially hydrolyzed PVA layer on the other side, not producing migration of PVA into the foodstuff but potentially preventing air and water vapor from going through the packaging material. While not bio-based, PVA is a biodegradable polymer and thus, when it comes to imparting barrier properties to paper, preferable to polyethylene laminates or synthetic waxes (Bayés et al. 2023; Paradossi et al. 2003).

With both DA-TOCNFs/AgNPs (food side) and PVA (air side), the air resistance of food packaging was over 300 s/100 mL and the average WVTR was  $325 \text{ g m}^{-2} \text{ d}^{-1}$ . Both fail short from the barrier

**Table 3** Physical, barrier, and mechanical properties of the material proposed in this work, compared to uncoated papers, as passive packaging

Material	Grammage (g m <sup>-2</sup> )	Thickness (μm)	WVTR (g m <sup>-2</sup> d <sup>-1</sup> )	Air resistance (s/100 mL)	Burst index (kPa m <sup>2</sup> g <sup>-1</sup> )	Tear index (mN m <sup>2</sup> g <sup>-1</sup> )	Tensile index (N m g <sup>-1</sup> )
Uncoated paper	170 ± 1	249 ± 1	1070 ± 60	29 ± 1	2.04 ± 0.08	10.0 ± 0.4	52 ± 5
DA-TOCNFs/ AgNPs – paper	172 ± 1	260 ± 4	Not measured	38 ± 8	2.17 ± 0.03	11.9 ± 0.5	50 ± 6
DA-TOCNFs/ AgNPs – paper – PVA	175 ± 1	278 ± 2	325 ± 12	302 ± 38	2.56 ± 0.12	13.3 ± 0.5	61 ± 8

properties of conventional plastic packaging, but the relative improvement was of one order of magnitude and three-fold, respectively.

Regarding the mechanical properties, there was significant enhancement of the tear and burst indices, but the confidence intervals of tensile properties (tensile index and strain at break) presented partial or even total overlapping ( $p > 0.05$ ). Plausible increases in burst resistance with PVA and CNF-based coatings, along with non-significant effects over the tensile strength, have been found in previous works (Mazega et al. 2022b).

One of the main concerns of the use of AgNP suspensions is the high mobility and diffusion of AgNPs, causing their inevitable ease of migration in liquid-based materials such as food, or cosmetic products. Given the concerns related to metallic nanoparticles in edible products (Schneider 2017), the immobilization of AgNPs on the cellulose fibrils, along with their effective binding on the paper surface, would reduce any likelihood risk of excessive migration of AgNPs from the paper packaging to the surrounding liquid. In the European Union, the Scientific Panel on food additives, flavourings, processing aids and materials in contact with food (AFC panel) sets a specific migration limit of 50 μg kg<sup>-1</sup> for silver (EFSA 2006). Out of the different food simulants, the one that attains the highest level of migration is aqueous acetic acid, *i.e.*, simulant B (Schneider 2017).

Interestingly, the resulting coated papers exhibited no silver migration after being in contact for 24 h in food simulant D1 (aqueous ethanol, 50 vol%), as ICP-OES revealed a silver concentration below the detection limit. In the case of food simulant B (aqueous acetic acid, 3 wt/vol%), some silver migration was detected, but it was as low as 3.2 ± 0.7 μg dm<sup>-2</sup>,

or 12.7 ± 3.0 μg kg<sup>-1</sup>. For DA-TOCNFs/AgNPs-5·10<sup>-2</sup> M, migration to food simulant B was 11.2 μg dm<sup>-2</sup> or 44.4 μg kg<sup>-1</sup>, still below the specific migration limit indicated by the EU's AFC panel (EFSA 2006). For simulant D1, the concentration of silver was undetectable. This is of particular interest for considering DA-TOCNFs/AgNPs as paper coating for food contact applications, as food safety would not be compromised. In fact, the attachment of AgNPs on the cellulose nanofibrils would prevent the leaching out and the release of AgNPs from the surface, which explains why AgNPs remained entrapped within the fibrillar network of the paper. This phenomenon would even be favored by the high aptitude of the cellulose nanofibrils to interact via hydrogen bonding with the cellulose fibers.

#### Antibacterial characteristics of DA-TOCNFs/AgNPs-coated papers

As described above, papers were coated using an automated bar coater. ICP-OES of the digested in nitric acid revealed that the amount of nanosilver incorporated onto the coated papers was not directly proportional to the concentration of the suspensions used for this purpose, possibly due to their different rheological properties. For instance, those attained with [Ag<sup>+</sup>] = 10<sup>-2</sup> M (using either DAC or DA-TOCNFs) resulted in papers with roughly 120 μg Ag/g, while those with [Ag<sup>+</sup>] = 0.1 M raised the silver content on paper to only 372 μg Ag/g, instead of tenfold. While antibacterial activity is equally expected from both DAC/AgNPs and DA-TOCNFs/AgNPs, this section focuses on the latter, due to the more efficient reduction of Ag<sup>+</sup>, to the successful silver-nanofibril binding, and to their higher degree of novelty.

The activity against Gram-positive *Bacillus subtilis* was observed macroscopically (Fig. S2c–f), by optical microscopy (Fig. 9), and by SEM (Fig. 10). Inhibition of *B. subtilis* growth on the surface of paper coated with DA-TOCNF/AgNPs- $10^{-2}$  M lasted for at least 30 days. However, the growth of *E. coli*, a Gram-negative bacteria, was not fully inhibited with this concentration. Figure S2 shows that *E. coli* colonized the surface of the paper disks, even if it was to a lesser extent than in the case of the blank sample. Due to the difficulty of counting colonies from the pictures, microbial growth over paper disks was evidenced by a brief exposure to white light. Paper hardly displayed white light reflectance, but colonies did (Reipa et al. 2006).

While *E. coli* is, like *B. subtilis*, widely reported to be susceptible to AgNPs, the latter was found to be more liable than the former, in line with a previous study (Yoon et al. 2007). The activity of AgNPs against *E. coli* is primarily mediated by the release of  $\text{Ag}^+$  ions, which trespass with relative ease through the outer membrane and the thin peptidoglycan cell wall of Gram-negative bacteria (Sotiriou et al. 2012; Ivask et al. 2014). It can be conjectured that DA-TOCNFs provided AgNPs with such stability that ion release was hampered. Furthermore, the growth around coated paper disks in Fig. S2 can be attributed to the release of PVA

to the medium, but it should be kept in mind that this layer is not meant to be in contact with food. For instance, without PVA and with more silver concentration, even inhibition halos were observed (Fig. S3). For the sake of effective growth inhibition besides the packaging itself, the recommended amount of AgNPs on paper sheets is roughly  $0.18 \text{ g/m}^2$ , corresponding to a Tollens' reagent concentration of 0.05 M (calculated from Fig. 6 for a coat weight of  $2 \text{ g/m}^2$ ).

The OM images, both from the uncoated (Fig. 9a series) and coated (Fig. 9b series), reveal the growth of *B. subtilis* at the surface of the non-treated testliner papers. This indicates that the activity against Gram-positive bacteria is low or inexistent, limiting the use of this paper for food contact applications. On the contrary, the coated paper exhibited a high activity against the bacteria, limiting the growth of any colony at the surface.

These colonies were also observed by SEM (Fig. 10), allowing for a significantly higher magnification, and providing a comprehensive understanding of the structure of such colonies, particularly as revealed by the third image (a3) from Fig. 10a. In the case of coated paper (Fig. 10b series), some colonies were also observed but, as indicated in yellow, the presence of AgNPs limited the growth of *B. subtilis* at the surface of paper, generating membrane damage into the bacteria.

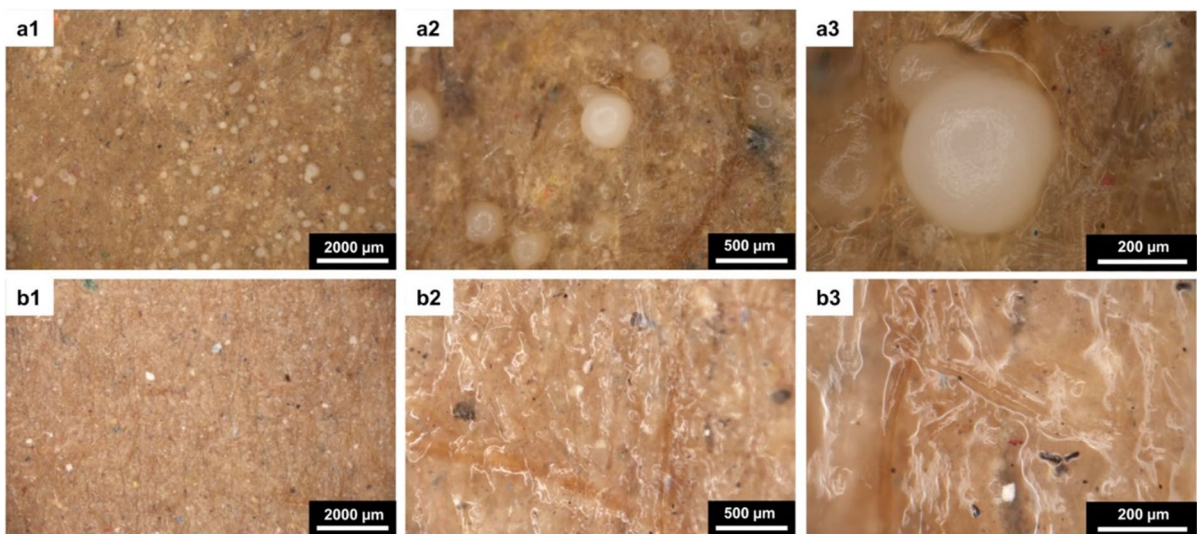


**Fig. 9** Optical microscopy images of the surface of uncoated paper (a1, a2, a3) and of paper coated with DA-TOCNFs/AgNPs- $10^{-2}$  M (b1, b2, b3), both inoculated with *B. subtilis*, at increasing magnification levels

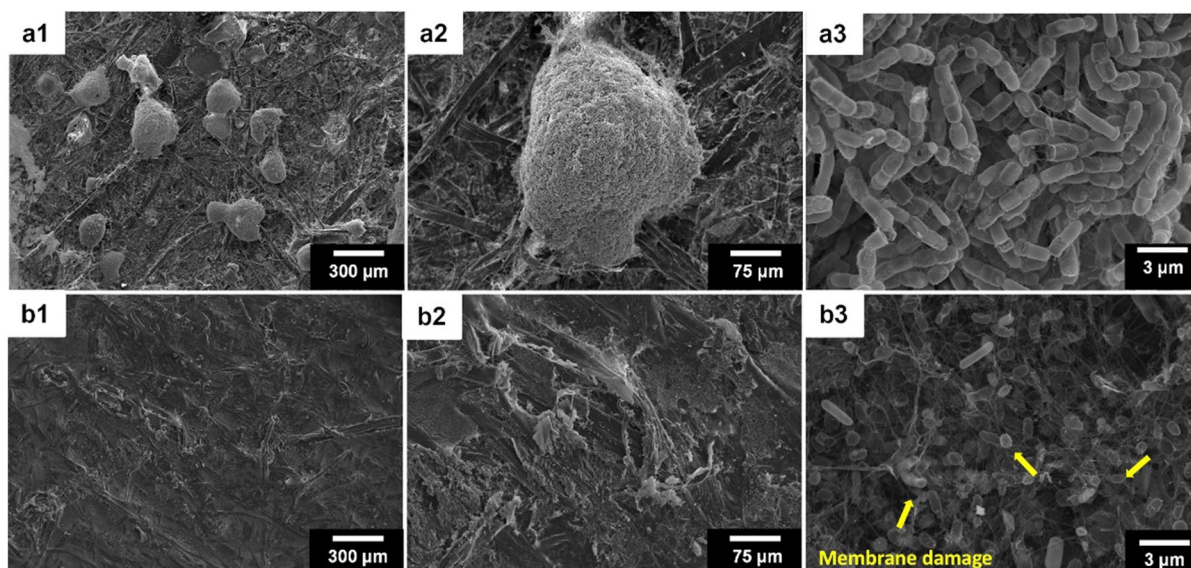


**Fig. 10** SEM images following *B. subtilis* growth on uncoated paper (**a1**, **a2**, **a3**) and of paper coated with DA-TOCNFs/AgNPs- $10^{-2}$  M (**b1**, **b2**, **b3**), at increasing magnification levels

Although the antibacterial effect of silver-based nanomaterials has been the subject of numerous reports and reviews, the mode of action of AgNPs and  $\text{Ag}^+$  ions released therefrom is still a matter of debate. It implicates multilevel mode of action, including the disruption of bacterial metabolic processes leading to the protein and DNA inactivation (Feng et al. 2000), increasing the cytoplasmic membrane permeability by the creation of cavities (Q. Li et al. 2008), and the generation of reactive oxygen species (ROS) that catalyze the destructive oxidation of microorganisms (Yoshinobu et al. 2003). From the chemical point of view, silver (either in the form of NPs or ionic species) possesses a very high affinity for organic amines, phosphates, and most notably thiols, with which they form a quasi-covalent bond, resulting in the inactivation of biological systems bearing these moieties by forming an irreversible adduct with them causing the cellular death.

## Conclusions

Stable suspensions of AgNPs and oxidized cellulosic derivatives were successfully produced. Aldehyde groups on the surface of the cellulose

derivatives worked simultaneously as reducer and binding sites. A remarkable finding of this work was that the coexistence of carboxylate and aldehyde groups improved both the nucleation of AgNPs and their binding to oxidized cellulose. This double oxidation (TEMPO-mediated and periodate oxidations) allowed for the nucleation of more AgNPs and for a more stable association. Such enhancement was attributed to a higher degree of repulsion between surfaces, e.g.: for  $[\text{Ag}^+] = 10^{-2}$  M, the  $\zeta$ -potential was  $-16$  mV in the case of DAC and  $-32$  mV in the case of DA-TOCNFs. Nonetheless, in both cases, the reduction of the Ag precursor was quick and the resulting AgNPs were not prone to aggregation. Finally, packaging paper sheets that were coated with these AgNP-containing suspensions displayed a clear antimicrobial activity, inhibiting the growth of *B. subtilis* over the food contact side and damaging their cell membranes. In order to enhance the gas barrier properties, the other side was coated with PVA, granting a ten-fold increase in air resistance and a three-fold decrease in WVTR.

Oxidized cellulose derivatives, especially DA-TOCNFs, did not only fulfill the role of reducing agent, but also the roles of stabilizer, support material for the nanoparticles, binder, and thickener. Stabilization prevented further aggregation of AgNPs,

which reached a limited size, and no unbound particles were identified. The resulting suspensions were proper for paper coating due to all of these effects.

**Acknowledgments** Authors wish to acknowledge the financial support of the funding agencies listed in the “Funding” section. Marc Delgado-Aguilar is a Serra Hünter Fellow.

**Authors’ contributions** Mohamed Aouay: Writing – Original Draft, Formal analysis, Investigation; Roberto J. Aguado: Conceptualization, Writing – Review & Editing; Genís Bayés: Investigation; Núria Fiol: Formal analysis, Investigation; Jean-Luc Putaux: Investigation, Writing – Original Draft; Sami Boufi: Conceptualization, Writing – Review & Editing, Project administration, Funding acquisition; Marc Delgado-Aguilar: Conceptualization, Writing – Review & Editing, Project administration, Funding acquisition. The manuscript was approved by all the authors.

**Funding** Open Access funding provided thanks to the CRUE-CSIC agreement with Springer Nature. The authors wish to acknowledge the Spanish Ministry of Science and Innovation for the financial support to the project NextPack (PID2021-124766OA-I00), the Government of Catalonia for the Industrial Doctorate project 2021 DI 13, which partially funds the PhD project of Genís Bayés, as well as the NanoBio-ICMG platform (UAR 2607, Grenoble) for granting access to the Electron Microscopy Facility.

**Data availability** No datasets were generated or analysed during the current study.

## Declarations

**Ethics approval and consent to participate** Authors declare that the manuscript is not submitted to any other journal at the time of submission for simultaneous consideration, that the submitted work is original and has not been published elsewhere in any form, that this work is not part of a single study, that results are presented under the principles of honesty, without fabrication or inappropriate data manipulation and that no data, text or theories by others are presented as our own.

**Consent for publication** The manuscript was read and approved by all the authors.

**Competing interests** The authors declare no competing interests.

**Open Access** This article is licensed under a Creative Commons Attribution 4.0 International License, which permits use, sharing, adaptation, distribution and reproduction in any medium or format, as long as you give appropriate credit to the original author(s) and the source, provide a link to the Creative Commons licence, and indicate if changes were made. The images or other third party material in this article are included in the article’s Creative Commons licence, unless indicated otherwise in a credit line to the material. If material is not

included in the article’s Creative Commons licence and your intended use is not permitted by statutory regulation or exceeds the permitted use, you will need to obtain permission directly from the copyright holder. To view a copy of this licence, visit <http://creativecommons.org/licenses/by/4.0/>.

## References

- Agarwal UP, Ralph SA, Baez C et al (2017) Effect of sample moisture content on XRD-estimated cellulose crystallinity index and crystallite size. *Cellulose* 24:1971–1984. <https://doi.org/10.1007/s10570-017-1259-0>
- Aguado R, Murtinho D, Valente AJM (2019) A broad overview on innovative functionalized paper solutions. *Nord Pulp Paper Res J* 34:395–416. <https://doi.org/10.1515/npprj-2019-0036>
- Aguado R, Murtinho D, Valente AJM (2021) Association of antioxidant monophenolic compounds with  $\beta$ -cyclodextrin-functionalized cellulose and starch substrates. *Carbohydr Polym* 267:118189. <https://doi.org/10.1016/j.carbpol.2021.118189>
- Amini E, Azadfallah M, Layeghi M, Taleai-Hassanloui R (2016) Silver-nanoparticle-impregnated cellulose nanofiber coating for packaging paper. *Cellulose* 23:557–570. <https://doi.org/10.1007/s10570-015-0846-1>
- Anthierens T, Ragaert P, Verbrugghe S et al (2011) Use of endospore-forming bacteria as an active oxygen scavenger in plastic packaging materials. *Innov Food Sci Emerg Technol* 12:594–599
- ASTM (2017) E96: standard test methods for water vapor transmission of materials. ASTM International
- Bastos-Arrieta J, Florido A, Pérez-Ráfols C, et al (2018) Green synthesis of Ag nanoparticles using grape stalk waste extract for the modification of screen-printed electrodes. *Nanomaterials* 8. <https://doi.org/10.3390/nano8110946>
- Bayés G, Aguado RJ, Tarrés Q, et al (2023) Stabilization of Beeswax-In-Water Dispersions Using Anionic Cellulose Nanofibers and Their Application in Paper Coating. *Nanomaterials* 13
- Boufi S, González I, Delgado-Aguilar M, et al (2016) Nanofibrillated cellulose as an additive in papermaking process: a review. *Carbohydr Polym* 154. <https://doi.org/10.1016/j.carbpol.2016.07.117>
- Brito BSL, Pereira FV, Putaux J-L, Jean B (2012) Preparation, morphology and structure of cellulose nanocrystals from bamboo fibers. *Cellulose* 19:1527–1536. <https://doi.org/10.1007/s10570-012-9738-9>
- Brodin FW, Gregersen ØW, Syverud K (2014) Cellulose nanofibrils: challenges and possibilities as a paper additive or coating material—a review. *Nord Pulp Paper Res J* 29:156–166
- Busolo MA, Fernandez P, Ocio MJ, Lagaron JM (2010) Novel silver-based nanoclay as an antimicrobial in polylactic acid food packaging coatings. *Food Addit Contam Part A Chem Anal Control Expo Risk Assess* 27:1617–1626. <https://doi.org/10.1080/19440049.2010.506601>
- Cael JJ, Koenig JL, Blackwell J (1974) Infrared and raman spectroscopy of carbohydrates. *Carbohydr Res*. [https://doi.org/10.1016/s0008-6215\(00\)82465-9](https://doi.org/10.1016/s0008-6215(00)82465-9)

- Chung C, Lee M, Choe EK (2004) Characterization of cotton fabric scouring by FT-IR ATR spectroscopy. *Carbohydr Polym* 58:417–420. <https://doi.org/10.1016/j.carbpol.2004.08.005>
- Commission E (2019) Directive (EU) 2019/904 of the European Parliament and of the Council of 5 June 2019 on the reduction of the impact of certain plastic products on the environment. Belgium, Brussels
- EFSA (2006) Opinion of the Scientific Panel on food additives, flavourings, processing aids and materials in contact with food (AFC) related to the 12th list of substances for food contact materials. *EFSA J* 4:395. <https://doi.org/10.2903/j.efsa.2006.395>
- Elamawi RM, Al-Harbi RE, Hendi AA (2018) Biosynthesis and characterization of silver nanoparticles using *Trichoderma longibrachiatum* and their effect on phytopathogenic fungi. *Egypt J Biol Pest Control* 28:1–11. <https://doi.org/10.1186/s41938-018-0028-1>
- Elazzouzi-Hafraoui S, Nishiyama Y, Putaux J-L et al (2008) The shape and size distribution of crystalline nanoparticles prepared by acid hydrolysis of native cellulose. *Biomacromol* 9:57–65. <https://doi.org/10.1021/bm700769p>
- Errokh A, Magnin A, Putaux J-L, Boufi S (2019) Hybrid nanocellulose decorated with silver nanoparticles as reinforcing filler with antibacterial properties. *Mater Sci Eng, C* 105:110044. <https://doi.org/10.1016/j.msec.2019.110044>
- Feng QL, Wu J, Chen GQ et al (2000) A mechanistic study of the antibacterial effect of silver ions on *Escherichia coli* and *Staphylococcus aureus*. *J Biomed Mater Res* 52:662–668. [https://doi.org/10.1002/1097-4636\(20001215\)52:4%3c662::AID-JBM10%3e3.0.CO;2-3](https://doi.org/10.1002/1097-4636(20001215)52:4%3c662::AID-JBM10%3e3.0.CO;2-3)
- Fortunati E, Armentano I, Zhou Q et al (2012) Multifunctional bionanocomposite films of poly(lactic acid), cellulose nanocrystals and silver nanoparticles. *Carbohydr Polym* 87:1596–1605. <https://doi.org/10.1016/j.carbpol.2011.09.066>
- Fortunati E, Rinaldi S, Peltzer M et al (2014) Nano-biocomposite films with modified cellulose nanocrystals and synthesized silver nanoparticles. *Carbohydr Polym* 101:1122–1133. <https://doi.org/10.1016/j.carbpol.2013.10.055>
- French AD (2014) Idealized powder diffraction patterns for cellulose polymorphs. *Cellulose* 21:885–896. <https://doi.org/10.1007/s10570-013-0030-4>
- French AD (2020) Increment in evolution of cellulose crystallinity analysis. *Cellulose* 27:5445–5448
- French AD, Santiago Cintrón M (2013) Cellulose polymorphy, crystallite size, and the Segal Crystallinity Index. *Cellulose* 20:583–588. <https://doi.org/10.1007/s10570-012-9833-y>
- Garza-Cervantes JA, Mendiola-Garza G, de Melo EM et al (2020) Antimicrobial activity of a silver-microfibrillated cellulose biocomposite against susceptible and resistant bacteria. *Sci Rep* 10:1–7. <https://doi.org/10.1038/s41598-020-64127-9>
- González I, Boufi S, Pèlach MA et al (2012) Nanofibrillated cellulose as paper additive in eucalyptus pulps. *BioResources* 7:5167–5180. <https://doi.org/10.15376/biores.7.4.5167-5180>
- Guo J, Catchmark JM (2012) Surface area and porosity of acid hydrolyzed cellulose nanowhiskers and cellulose produced by *Gluconacetobacter xylinus*. *Carbohydr Polym* 87:1026–1037. <https://doi.org/10.1016/j.carbpol.2011.07.060>
- He Y, Li H, Fei X, Peng L (2021) Carboxymethyl cellulose/cellulose nanocrystals immobilized silver nanoparticles as an effective coating to improve barrier and antibacterial properties of paper for food packaging applications. *Carbohydr Polym* 252. <https://doi.org/10.1016/j.carbpol.2020.117156>
- Hii C, Gregersen Ø, Chinga-Carrasco G, Eriksen Ø (2012) The effect of MFC on the pressability and paper properties of TMP and GCC based sheets. *Nord Pulp Paper Res J* 27:388–396. <https://doi.org/10.3183/NPPRJ-2012-27-02-p388-396>
- Hosseinidou Z, Basnet M, van de Ven TGM, Tufenkji N (2016) One-pot green synthesis of anisotropic silver nanoparticles. *Environ Sci Nano* 3:1259–1264. <https://doi.org/10.1039/C6EN00112B>
- Hubbe MA, Ferrer A, Tyagi P et al (2017) Nanocellulose in thin films, coatings, and plies for packaging applications: a review. *BioResources* 12:2143–2233
- Hult E-L, Iotti M, Lenis M (2010) Efficient approach to high barrier packaging using microfibrillar cellulose and shellac. *Cellulose* 17:575–586
- Ifuku S, Tsuji M, Morimoto M et al (2009) Synthesis of silver nanoparticles templated by TEMPO-mediated oxidized bacterial cellulose nanofibers. *Biomacromol* 10:2714–2717
- ISO (2011) ISO TC/6: Paper, board and pulps. International standardization organization, Geneva (Switzerland)
- Ivask A, ElBadawy A, Kaweeterawat C et al (2014) Toxicity mechanisms in *Escherichia coli* vary for silver nanoparticles and differ from ionic silver. *ACS Nano* 8:374–386. <https://doi.org/10.1021/nn4044047>
- Jung J, Raghavendra GM, Kim D, Seo J (2018) One-step synthesis of starch-silver nanoparticle solution and its application to antibacterial paper coating. *Int J Biol Macromol* 107:2285–2290
- Karami C, Taher MA (2018) Colorimetric sensor of cobalt ions in aqueous solution using gold nanoparticles modified with glycyrrhizic acid. *Plasmonics*. <https://doi.org/10.1007/s11468-017-0635-9>
- Khwaldia K (2010) Water vapor barrier and mechanical properties of paper-sodium caseinate and paper-sodium caseinate-paraffin wax films. *J Food Biochem* 34:998–1013
- Kljun A, Benians TAS, Goubet F et al (2011) Comparative analysis of crystallinity changes in cellulose I polymers using ATR-FTIR, X-ray diffraction, and carbohydrate-binding module probes. *Biomacromol* 12:4121–4126. <https://doi.org/10.1021/bm201176m>
- Kolya H, Hashitume K, Kang C-W (2022) Ammonium persulfate treatment on carbohydrate polymers and lignin of wood improved sound absorption capacity. *Int J Biol Macromol* 205:626–637. <https://doi.org/10.1016/j.ijbiomac.2022.02.075>
- Kumar V, Elfving A, Koivula H et al (2016) Roll-to-roll processed cellulose nanofiber coatings. *Ind Eng Chem Res* 55:3603–3613. <https://doi.org/10.1021/acs.iecr.6b00417>
- La Spina R, Mehn D, Fumagalli F et al (2020) Synthesis of citrate-stabilized silver nanoparticles modified by thermal

- and ph preconditioned tannic acid. *Nanomaterials* 10:1–16. <https://doi.org/10.3390/nano10102031>
- Lavoine N, Desloges I, Dufresne A, Bras J (2012) Microfibrillated cellulose - Its barrier properties and applications in cellulosic materials: a review. *Carbohydr Polym* 90:735–764. <https://doi.org/10.1016/j.carbpol.2012.05.026>
- Li J, Kang L, Wang B et al (2018) Controlled release and long-term antibacterial activity of dialdehyde nanofibrillated cellulose/silver nanoparticle composites. *ACS Sustain Chem Eng* 7:1146–1158
- Li J, Kang L, Wang B et al (2019) Controlled release and long-term antibacterial activity of dialdehyde nanofibrillated cellulose/silver nanoparticle composites. *ACS Sustain Chem Eng* 7:1146–1158. <https://doi.org/10.1021/acsschemeng.8b04799>
- Li Q, Mahendra S, Lyon DY et al (2008) Antimicrobial nanomaterials for water disinfection and microbial control: potential applications and implications. *Water Res* 42:4591–4602. <https://doi.org/10.1016/j.watres.2008.08.015>
- Link S, El-Sayed MA (1999) Spectral properties and relaxation dynamics of surface plasmon electronic oscillations in gold and silver nanodots and nanorods. *J Phys Chem B* 103:8410–8426. <https://doi.org/10.1021/jp9917648>
- Lou T, Chen L, Chen Z et al (2011) Colorimetric detection of trace copper ions based on catalytic leaching of silver-coated gold nanoparticles. *ACS Appl Mater Interfaces*. <https://doi.org/10.1021/am2008486>
- Lu P, Zhao H, Zheng L et al (2022) Nanocellulose/nisin hydrogel microparticles as sustained antimicrobial coatings for paper packaging. *ACS Appl Polym Mater* 4:2664–2673
- Mazega A, Tarrés Q, Aguado R, et al (2022a) Improving the barrier properties of paper to moisture, air, and grease with nanocellulose-based coating suspensions. *Nanomaterials* 12. <https://doi.org/10.3390/nano12203675>
- Mazega A, Tarrés Q, Aguado R et al (2022b) Improving the barrier properties of paper to moisture, air, and grease with nanocellulose-based coating suspensions. *Nanomaterials* 12:3675. <https://doi.org/10.3390/nano12203675>
- Mehdaoui R, Agren S, Dhahri A et al (2021) New sonochemical magnetite nanoparticles functionalization approach of dithiooxamide–formaldehyde developed cellulose: From easy synthesis to recyclable 4-nitrophenol reduction. *Appl Organomet Chem* 35:e6257. <https://doi.org/10.1002/aoc.6257>
- Mu H, Gao H, Chen H et al (2013) A nanosized oxygen scavenger: preparation and antioxidant application to roasted sunflower seeds and walnuts. *Food Chem* 136:245–250
- Paradossi G, Cavalieri F, Chiessi E, Spagnoli C, Cowman MK (2003) Poly(vinyl alcohol) as versatile biomaterial for potential biomedical applications. *J Mater Sci: Mater Med* 14(8):687–691
- Pawcenis D, Chlebda DK, Jędrzejczyk RJ et al (2019) Preparation of silver nanoparticles using different fractions of TEMPO-oxidized nanocellulose. *Eur Polym J* 116:242–255. <https://doi.org/10.1016/j.eurpolymj.2019.04.022>
- Rastogi VK, Samyn P (2015) Bio-based coatings for paper applications. *Coatings* 5:887–930. <https://doi.org/10.3390/coatings5040887>
- Reipa V, Almeida J, Cole KD (2006) Long-term monitoring of biofilm growth and disinfection using a quartz crystal microbalance and reflectance measurements. *J Microbiol Methods* 66:449–459. <https://doi.org/10.1016/j.mimet.2006.01.016>
- Schneider G (2017) Antimicrobial silver nanoparticles – regulatory situation in the European Union. *Mater Today Proc* 4:S200–S207. <https://doi.org/10.1016/j.matpr.2017.09.187>
- Segal L, Creely JJ, Martin AE, Conrad CM (1959) An empirical method for estimating the degree of crystallinity of native cellulose using the x-ray diffractometer. *Text Res J* 29:786–794. <https://doi.org/10.1177/004051755902901003>
- Serra A, González I, Oliver-Ortega H, et al (2017) Reducing the amount of catalyst in TEMPO-oxidized cellulose nanofibers: Effect on properties and cost. *Polymers (Basel)* 9. <https://doi.org/10.3390/polym9110557>
- Serra-Parareda F, Aguado R, Tarrés Q et al (2021) Potentiometric back titration as a robust and simple method for specific surface area estimation of lignocellulosic fibers. *Cellulose* 28:10815–10825. <https://doi.org/10.1007/s10570-021-04250-6>
- Shaaban MT, Ghaly MF, Fahmi SM (2021) Antibacterial activities of hexadecanoic acid methyl ester and green-synthesized silver nanoparticles against multidrug-resistant bacteria. *J Basic Microbiol* 61(6):557–568
- Shalaby TI, Fekry NM, El SAS et al (2015) Preparation and characterisation of antibacterial silver-containing nanofibres for wound healing in diabetic mice. *Int J Nanoparticles* 8:82. <https://doi.org/10.1504/IJNP.2015.070346>
- Smitha SL, Nissamudeen KM, Philip D, Gopchandran KG (2008) Studies on surface plasmon resonance and photoluminescence of silver nanoparticles. *Spectrochim Acta A Mol Biomol Spectrosc* 71:186–190. <https://doi.org/10.1016/j.saa.2007.12.002>
- Sotiriou GA, Meyer A, Knijnenburg JTN et al (2012) Quantifying the origin of released Ag<sup>+</sup> ions from nanosilver. *Langmuir* 28:15929–15936. <https://doi.org/10.1021/la303370d>
- Tarrés Q, Boufi S, Mutjé P, Delgado-Aguilar M (2017) Enzymatically hydrolyzed and TEMPO-oxidized cellulose nanofibers for the production of nanopapers: morphological, optical, thermal and mechanical properties. *Cellulose* 24:3943–3954. <https://doi.org/10.1007/s10570-017-1394-7>
- Tarrés Q, Oliver-Ortega H, Ferreira PJ et al (2018) Towards a new generation of functional fiber-based packaging: cellulose nanofibers for improved barrier, mechanical and surface properties. *Cellulose* 25:683–695. <https://doi.org/10.1007/s10570-017-1572-7>
- Tyagi P, Hubbe MA, Lucia L, Pal L (2018) High performance nanocellulose-based composite coatings for oil and grease resistance. *Cellulose* 25:3377–3391. <https://doi.org/10.1007/s10570-018-1810-7>
- Tyagi P, Lucia LA, Hubbe MA, Pal L (2019) Nanocellulose-based multilayer barrier coatings for gas, oil, and grease resistance. *Carbohydr Polym* 206:281–288. <https://doi.org/10.1016/j.carbpol.2018.10.114>

- Uddin KMA, Lokanathan AR, Liljeström A et al (2014) Silver nanoparticle synthesis mediated by carboxylated cellulose nanocrystals. *Green Mater* 2:183–192
- Varma AJ, Chavan VB (1995) Thermal properties of oxidized cellulose. *Cellulose* 2:41–49. <https://doi.org/10.1007/BF00812771>
- Wang MS, Jiang F, Hsieh Y-L, Nitin N (2014) Cellulose nanofibrils improve dispersibility and stability of silver nanoparticles and induce production of bacterial extracellular polysaccharides. *J Mater Chem B* 2:6226–6235
- Wei J, Du C, Liu H et al (2016) Preparation and characterization of aldehyde-functionalized cellulosic fibers through periodate oxidation of bamboo pulp. *Bioresources* 11:8386–8395. <https://doi.org/10.15376/biores.11.4.8386-8395>
- Xu Q, Jin L, Wang Y et al (2019) Synthesis of silver nanoparticles using dialdehyde cellulose nanocrystal as a multi-functional agent and application to antibacterial paper. *Cellulose* 26:1309–1321. <https://doi.org/10.1007/s10570-018-2118-3>
- Yeo JH, Lee CH, Park C et al (2001) Rheological, morphological, mechanical, and barrier properties of PP/EVOH blends. *Adv Polym Technol: J Polym Process Inst* 20:191–201
- Yoon K-Y, HoonByeon J, Park J-H, Hwang J (2007) Susceptibility constants of *Escherichia coli* and *Bacillus subtilis* to silver and copper nanoparticles. *Sci Total Environ* 373:572–575. <https://doi.org/10.1016/j.scitotenv.2006.11.007>
- Yoshinobu M, Kuniaki Y, Shin-ichi K, Tetsuaki T (2003) Mode of bactericidal action of silver zeolite and its comparison with that of silver nitrate. *Appl Environ Microbiol* 69:4278–4281. <https://doi.org/10.1128/AEM.69.7.4278-4281.2003>
- Zeng J, Xiong X, Hu F, et al (2023) Dialdehyde cellulose solution as reducing agent: preparation of uniform silver nanoparticles and in situ synthesis of antibacterial composite films with high barrier properties. *Molecules* 28. <https://doi.org/10.3390/molecules28072956>
- Zhang X, Sun H, Tan S et al (2019) Hydrothermal synthesis of Ag nanoparticles on the nanocellulose and their antibacterial study. *Inorg Chem Commun* 100:44–50. <https://doi.org/10.1016/j.inoche.2018.12.012>

**Publisher's Note** Springer Nature remains neutral with regard to jurisdictional claims in published maps and institutional affiliations.